J Mater Sci: Mater Electron **(2024) 35:1540**

Variable range hopping conductivity of hydrothermally reduced graphene oxide fibers

Adam Ostrowski[1], Karol Synoradzki[1], Damian Tomaszewski[1], and Krzysztof Tadyszak[2,*]

[1] *Institute of Molecular Physics, Polish Academy of Sciences, Ul. Smoluchowskiego 17, 60-179 Poznan, Poland*
[2] *Institute of Macromolecular Chemistry CAS, Heyrovského Nám. 2, 162 06 Prague 6, Czech Republic*

Received: 5 April 2024
Accepted: 27 July 2024
Published online: 8 August 2024

ABSTRACT

We report applying the autoclaved hydrothermal method for obtaining conductive reduced graphene oxide (rGO) fibers for potential flexible electronic applications, such as supercapacitors, transistors, or sensing applications. The reduction of GO was performed in the temperature range 120 to 180 °C under increased pressure of ca. 8 bar in a sealed Teflon lined up, stainless steel autoclave. The fiber's diameter and length were defined by the glass tube used as the mold for reducing GO water suspension (diameter of 600 µm and length of 8 cm). After drying, in an ambient atmosphere, the hydrogel fiber shrinks to ca. 50 µm in diameter and 6 cm in length (collapsed pore structure). The drying process, in addition to enhancing electrical conductivity, also increases the mechanical strength of the fibers due to the stronger overlapping of the graphene flakes. The best performance was observed in the fiber reduced at the highest temperature studied, 180 °C, and a minimum temperature of 120 °C is necessary to obtain a fiber. Electrical conductivity was measured using the 4-probe method. The results were analyzed within the framework of variable range hopping and Arrhenius models to pinpoint the best model describing electrical conductivity in dry rGO fibers.

1 Introduction

Graphene oxide (GO) is the oxidized form of graphene having different types of oxygen groups on its surface (–COOH, –OH, =O, O=C–H–, –O–) [1]. Due to the material's properties, it is accessible to various chemical modifications. It is an electric isolator in the oxidized form, but electrical conductivity can be partially restored after the reduction – removal of oxygen groups. Such material can be applied in multiple fields, e.g., flexible electronics, especially in the form of fibers as electrical wires [2, 3], mechanical energy harvesters [4], sensors [5] (e.g., pressure [6], magnetic field [7], oxygen [8]), supercapacitors [9], FET transistors [10] it can be used in biomedicine [11], as cell scaffolds [12]. This article focuses on the electrical properties of rGO fibers obtained via the hydrothermal method in an autoclave at various temperatures. In general, the conductivity of such aerogel structures strongly depends on the pore structure, e.g., pore size, flakes overlapping/connections, moisture content [13, 14], remaining oxygen groups, quality of crystallographic

Address correspondence to E-mail: tadyszak@imc.cas.cz

https://doi.org/10.1007/s10854-024-13274-0

structure (low concentration of structural defects), the distance between graphene layers [15]. The mentioned parameters can be modified using reducing agents, e.g., hydrazine hydrate and hydroiodic acid, etc. [15]. The same material parameters influence magnetic properties, which we reported previously, e.g., electron paramagnetic resonance (EPR) of conduction electrons [16] (Dyson line shape [17]), EPR relaxation times [18], defects [19], manganese residue which contaminates the material after using Hummer's method for graphene oxidation [20].

The electrical conductivity mechanism of carbon-like samples, e.g., rGO, composites, and HOPG, is usually considered variable range hopping. In this model, some activation energy is necessary for electrical transport. The literature discrepancy is in the value of the power (β) that changes qualitatively the applied model. In the literature [21], both values $\beta = 1/3$, Mott VRH for 2D systems [22], and $\beta = 1/2$ for Efros-Shklovskii VRH [23, 24] can be found. We address these issues in this article by trying to find the best model to describe our findings.

2 Materials and methods

2.1 Graphene oxide

Graphene oxide was purchased from the NANOPOZ company (Poznan, Poland). Lateral flake size dispersion was in the range of 0.9–46 μm, with the maximum number of flakes with a diameter of ~ 2 μm obtained. Additional details can be found in the previous report [25].

2.2 Reduced graphene oxide fiber preparation

Briefly, 4 mg/ml suspension was injected to both-sided opened capillaries ID: 0.6 mm sealed with Teflon both sided placed in an autoclave and heated for two hours in various temperatures ranging from 120 to 180 °C in steps of 10 °C. Further, the sample obtained at 180°C was selected for studies. After obtaining hydrogel fibers, they were left to dry in an ambient atmosphere at 21 °C.

2.3 Energy-dispersive X-ray spectroscopy (EDX)

EDX measurements (5kV, Scanning Electron Microscope Jeol 7001TTLS), with quantitative calibration performed on silica nanoparticles, confirmed the partial reduction process ca. C: 79%w., O: 21%w. from initial C:56% and O:44% for GO flakes.

2.4 Vibrating sample magnetometry (VSM)

DC magnetic susceptibility measurements were performed using a Physical Properties Measurement System (PPMS) from Quantum Design (San Diego, CA, USA) equipped with vibrating sample magnetometry (VSM). Zero-Field-Cooled (ZFC) and Field-Cooled (FC) curves were taken in the temperature range from 4 to 300 K in the magnetic field of 0.3 T (3 kOe).

2.5 AC electric conductivity measurements

Conductivity measurements were performed with 4284A Hewlett Packard (20 Hz–1 MHz) Precision LCR Meters with the LakeShore 340 Temperature Controller. The conductivity measurements were performed in a nitrogen environment at a cooling rate of 1 K/min in the temperature range of 300–423 K. The fibers were attached to the contacts with a silver paste.

Before the proper measurement, the fibers were annealed at 385 K to remove residual water and solvent from the silver paste. Annealing was carried out until stable conductivity values were obtained as a function of time.

2.6 DC electric conductivity measurements

DC electric conductivity was obtained from the 4-probe method using the Physical Property Measurement System (PPMS) from Quantum Design (San Diego, CA, USA). The measurement was performed using the 4-probe method. The electrodes were made of silver wires with a diameter of 50 μm and attached to the samples with silver paste. Measurements were done in the range of 20–380 K in the presence of a magnetic field (0.5 and 1 T) and without a magnetic field.

3 Results and discussion

Reduced graphene oxide fibers were obtained due to the reduction of water suspension of graphene oxide (Fig. 1a). GO flake's lateral diameters were in the range of 0.9–46 μm, with a maximum size distribution at ~ 2 μm (Fig. 1a). The presence of monolayered rGO was confirmed by atomic force microscopy (data presented previously [25]).

GO water suspension was placed in glass tubes in a Teflon-lined autoclave. Hydrogel fiber was obtained after 2h of hydrothermal reduction (temperature 120–180 °C, and pressure ca. 8 bar). The reduction process binds the flakes together by Van der Waals forces and unsaturated bonds that appear during the removal of oxygen-reach groups. This process is more efficient at higher temperatures and for longer durations.

Hydrogel means that the pores of the fiber structure are filled by water, which remains after synthesis. After drying in an ambient atmosphere (21 °C), the water evaporates, and during this process, pores collapse. This results in a significant decrease in fiber diameter from an initial 600 μm to ca. 50 μm and a slight decrease in the fiber length by roughly 20%. Dried fiber could be placed in a scanning electron microscope, and further composition measurements (EDX) could be performed. The EDX measurement was performed on a ca. 150 μm × 200 μm (5 kV) surface. It showed a reduction of oxygen groups compared with the initial GO sample (Fig. 1b). The flake arrangement is visible in a scanning electron microscope (Fig. 1b, c). The pore structure of the fibers presented here, previously revealed with focused ion beam etching (FIB), can be found under the reference [26], and CT, MRI, and EPRI images of aerogels which were obtained by the same method can be found here [27].

There are three methods of gel drying: critical point drying, lyophilization or freeze drying, and drying in an ambient atmosphere. The first two preserve the pore sizes, so the aerogel obtained is extremely fragile [25] but simultaneously has a large volume-to-mass ratio. Due to the drying in the ambient atmosphere, evaporating water causes tension on pore walls, leading to their collapse. This causes the flakes to overlap more tightly, making the fiber harder and able to withstand larger tensile forces. To put it into perspective, grabbing fibers with tweezers without breaking them is now possible.

We have estimated the minimum temperature at which the hydrogel in the form of continuous 8 cm long fiber is formed. Loosely connected, barely reduced fibers appeared at 120 °C (393 K). This is also the minimum temperature at which the reduction of oxygen groups starts in the autoclave. Figure 2 shows higher resistivity in comparison to the resistivity of the fiber obtained at 130 °C. The resistivity decreases by 4.75 times between 120 and 130 °C. In the entire temperature range, resistivity decreases by 19.6 times.

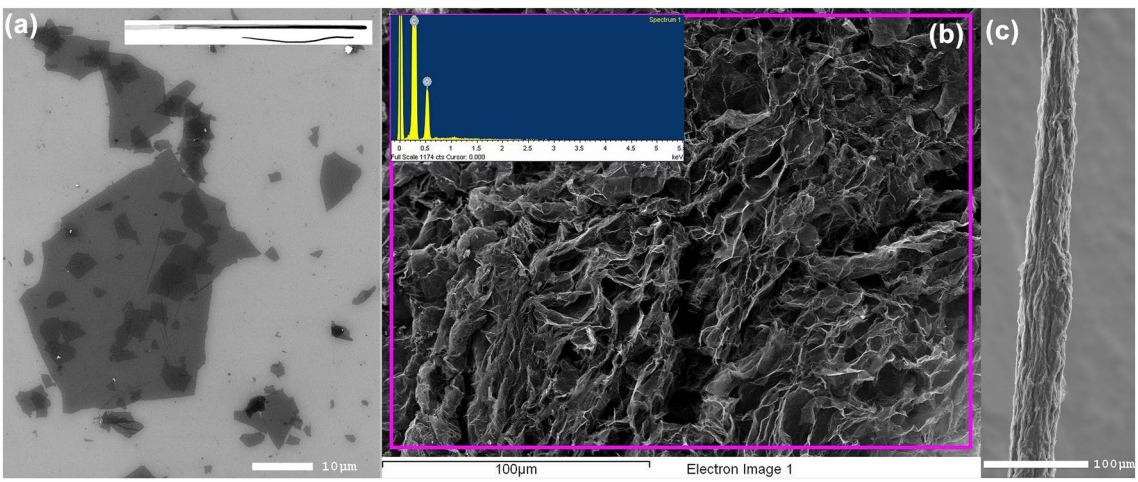

Fig. 1 **a** Scanning electron micro-image of GO flakes on Si surface; **b** SEM image of rGO fiber surface; violet square marks area from which data for EDX was collected in a pattern of 3 × 8 points measurements; (inset) EDX spectrum of the selected area; **c** low magnification SEM image of reduced graphene oxide fiber

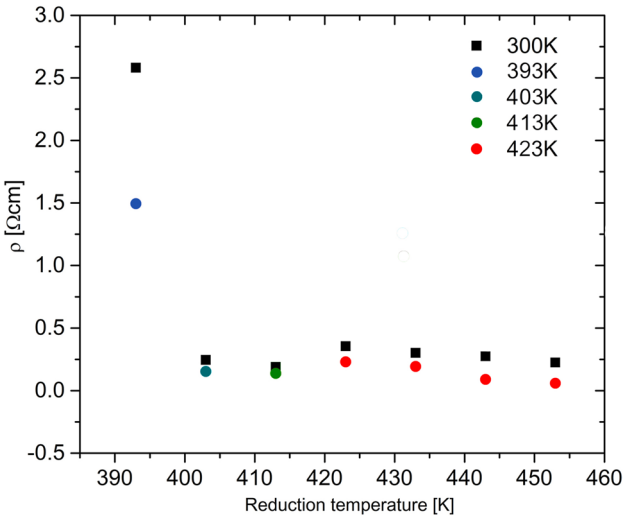

Fig. 2 Electrical resistivity was measured at 300 K (before drying) and at a higher temperature, as marked in Legend. The x-axis shows reduction temperatures for individual samples 120, 130, 140, 150, 160, 170, and 180 °C

In general, higher temperatures and longer reduction times improve conductivity. For partially reduced graphene oxide aerogel, it was 0.017 S/cm (180 °C, 2h) [28]; after 15 min. reductions at 220 °C conductivity increased to 2.64 S/cm, and for 2h reduction, it further increased to 4.6 S/cm [7]. Increasing the temperature to 800 °C for 4h resulted in conductivity of the order 85.2 S/cm [28]. Additional chemical reduction agents can speed up this process.

In general, the conductivity of hydrothermally synthesized graphene (temp. ~ 200 °C) fibers measured with the four-probe method at room temperature is ≤ 5 S/cm [29, 30], while by applying chemical reduction agents the process can be significantly improved [31]; after using $NaBH_4$ reducing agent conductivity raised to 214 S/cm [32], hydrazine reduction with aromatic molecules 13.9 S/cm (after annealing at 1000 °C it reaches 1314 S/cm) [33], site-selective functionalization (after annealing at 800 °C 1716 S/cm) [34]. Meanwhile, starting GO material shows conductivity for a single GO flake of the order 0.0005—2 S/cm [26], and for GO paper, due to loose flake stacking and a vast amount of oxygen groups, it is 1.2×10^{-6} S/cm [26].

RGO fiber's conductivity strongly depends on humidity and pore water content. An increase in conductivity from initial 10^{-6} up to 10^{-3} S/cm in GO films was observed while increasing relative humidity from 0 to 80% [13]. In this case, the conductivity of moist rGO films presented mixed electron-proton conductivity due to the admixture of ion conductivity of the water entrapped in pores [13]. Additionally, it was observed that under a relative humidity of 95%, the interlayer spacing increases from 0.368 to 0.380 nm [14]. Water penetration into the pores is slow and may take a few days [14]. Knowing this, our samples were dried before measurement until resistivity changes were not visible.

Figure 2 shows two sets of data. The first set consists of resistivity measurements done at room temperature (black squares) for samples reduced at 120, 130, 140, 150, 160, 170, and 180 °C. The second set consists of resistivity measurements on the same samples after drying at elevated temperatures (various drying temperatures marked with different circle colors). Resistivity measurements started only after stable resistivity measurements were reached. Due to the small fiber size, drying took ca. 2h. If drying was performed at a higher temperature than the reduction temperature, the oxygen removal process would continue changing the resistivity not because of water removal but oxygen removal instead, which we wanted to avoid.

Except for the first sample reduced at 120 °C (393 K), all others show similar resistivity values with a slight decrease towards high 180 °C (463 K). The first fiber shows the most significant difference in resistivity between room temperature and after drying, suggesting larger pores, loose flake arrangement, and, in general, more extensive water content. The last sample, due to the lowest resistivity and highest reduction temperature, was chosen for further electrical conductivity studies. Figure 3 presents the DC electrical conductivity (4-probe method) results for two fibers obtained at 180 °C. The resistivity vs. temperature $\rho(T)$ plot shows an exponential increase in resistivity while decreasing temperature. Both samples show identical temperature behavior. The nominal difference in resistivity is due to the spread of parameters caused by variations in pore structure and diameter changes along the fiber. Both fibers were measured in 0, 0.5, and 1 T. No magnetic field dependence on resistivity was found. Within the 20–380 K temperature range, resistivity increases around 2740 times. The increase in resistivity suggests an activation energy mechanism of electrical conductivity. This dependence is expected for a hopping-type mechanism of electrical

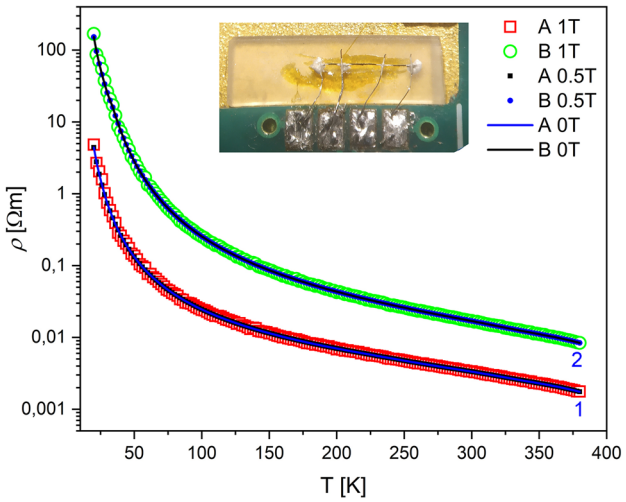

Fig. 3 Temperature dependence of DC electrical resistivity $\rho(T)$, measured with the four-probe method in the external magnetic field of 0, 0.5, and 1 T for two selected rGO fibers obtained after reduction at 180 °C and drying (labeled as A and B). Labels 1 and 2 correspond to the description in Table 1. The inset shows a photograph of a sample with electrodes attached and mounted on a measuring puck

conductivity, which involves temperature-activated tunneling processes between two localized states [22, 35].

Figure 4 shows electrical conductivity, which is the reverse of the data in Fig. 3 ($\sigma = \frac{1}{\rho}$). Multiple attempts were undertaken to find the model that describes these data well. The result of these valuations is summarized in Table 1. Exponential dependence can be fit by applying a general equation $\sigma = A \times exp\left(-\frac{T_0}{T}\right)^{\beta}$ where the fitting parameters are A—conductivity limit in high temperature [S/m], T_0—activation energy [K], and $\beta = (n-1)^{-1}$ is the dimensionality of the sample. After performing multiple fits by varying the parameter β, we have obtained results presented in Table 1.

The curves utilizing parameters from Table 1 are shown in Fig. 4a and b. The best fits showing the highest R^2 parameter were obtained using two conductivity mechanisms, described by the equation $A \bullet exp\left(-\frac{T_{0A}}{T}\right)^{0.5} + B \bullet exp\left(-\frac{T_{0B}}{T}\right)^{0.(3)}$ with β equal to 1/2 and 1/3 (Fig. 4a, Table 1). The first mechanism—Mott VRH ($\beta = 1/3$), with lower T_0 temperature, is dominant at lower temperatures [22], while the second mechanism—Efros-Shklovskii VRH ($\beta = ½$), activates at higher temperatures [23, 24]. Both models were observed in carbon-type samples [36]. Results from Table 1 are depicted in Fig. 4 a, b. A logarithmic scale is used to depict fitting errors clearly; in a linear scale, fits strongly overlap with data, providing less insight.

Table 1 Best fit parameters for multiple models

Function	Curve no (Fig. 3)	A, B [S/m]	SD—A, B [S/m]	T_0 [K]	SD—T_0 [K]	β	SD—β	Adj. R^2	Red. χ^2
$A \bullet exp\left(-\frac{T_0}{T}\right)^{0.25}$	1	2039	88	2183.9	52.4	0.25	0	0.9704	692.28
	2	682.4	26.2	2836.2	48.7	0.25	0	0.9855	15.557
$A \bullet exp\left(-\frac{T_0}{T}\right)^{0.(3)}$	1	2039.4	87.7	1638.0	39.3	0.(3)	0	0.9704	692.28
	2	682.4	26.2	2127.2	36.5	0.(3)	0	0.9855	15.557
$A \bullet exp\left(-\frac{T_0}{T}\right)^{0.5}$	1	2039.6	87.7	1092.0	26.2	0.5	0	0.9704	692.28
	2	682.4	26.2	1418.1	24.3	0.5	0	0.9855	15.557
$A \bullet exp\left(-\frac{T_{0A}}{T}\right)^{0.5}$	1	(A) 34819.2	2686.4	3628.9	64.5	0.5	0	0.9994	14.203
		(B) 519.8	11.5	785.3	11.0	0.(3)	0		
$+B \bullet exp\left(-\frac{T_{0B}}{T}\right)^{0.(3)}$	2	(A) 11049.8	859.2	4001.3	67.7	0.5	0	0.9997	0.2931
		(B) 171.0	4.3	1202.5	13.6	0.(3)	0		

Function	Curve no. Fig. 3	ρ_0	SD—ρ_0	T_0 [K]	SD—T_0 [K]	B	SD—B	Adj. R^2	Red. χ^2
$\rho(T) = \rho_0 \bullet exp\left(B\frac{T_0 - T}{T_0 T}\right)$	1	473.8	4.1×10^7	11	0.8	112.6	8.96×10^4	0.9959	7.6×10^{-4}
	2	2270.8	5.1×10^7	13.7	1.2	115.8	1.00×10^5	0.9924	1.6856

Data taken from Fig. 3

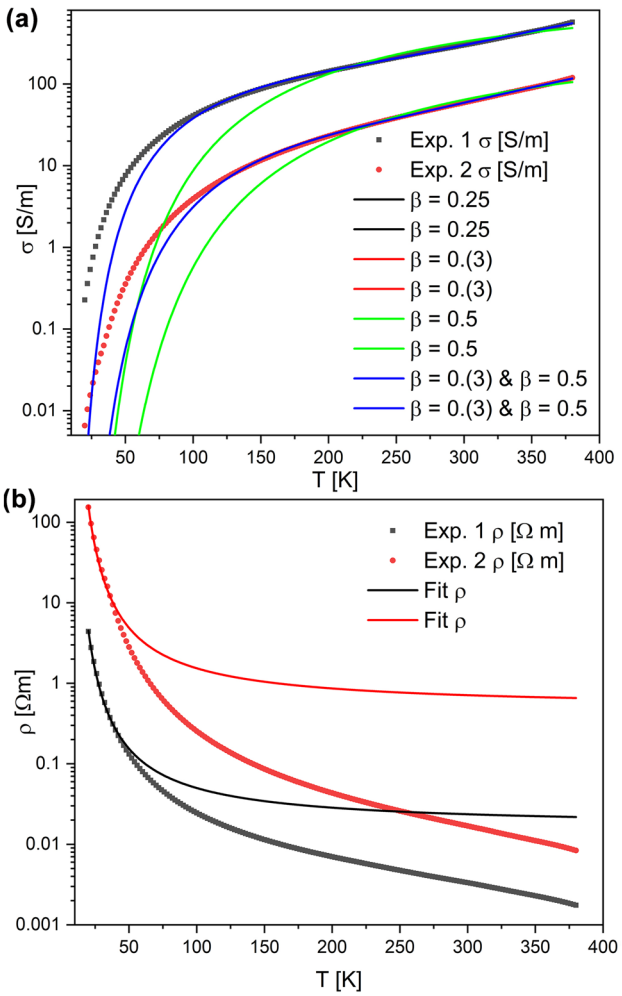

Fig. 4 The logarithm of DC conductivity (**a**) and resistivity (**b**) as a function of temperature; the sample was reduced to 180 °C. The data labeled 1 and 2 ($\mu_0 H = 0$ T) are taken from Fig. 3. The solid lines represent fits derived from different models presented in Table 1

It is visible that VRH models have trouble matching the data at lower temperatures. In both cases in Fig. 4a, the curves for $\beta = 0.25$; 0.(3); 0.5 are overlapping.

In literature, a different empirical equation describing temperature dependence on resistance of rGO can be found [37] utilizing Arrhenius-type dependence. In this case, the following equation was used: Where $\rho(T)$ is the resistance, ρ_0 is reference resistance in the highest studied temperature, T_0 is temperature, and B is the coefficient, which for conventional metal oxides is in the range 2000 to 5000 K (in ref. [38], it was 1860 K in our case only 150 K). This dependence was generally used for materials exhibiting negative temperature coefficients and exponential resistance dependence. In contrast to previous models, this one shows the most significant errors at higher temperatures.

The DC electron resistivity is equal to 4.8 and 168 Ωm at 20 K and goes down to 0.0034 and 0.017 Ωm at 300 K (Fig. 4), while the DC component taken from AC conductivity measurements (Fig. 5 inset) is at 300 K equal to 0.0054 Ωm and decreases with the increase of temperature to 0.0037 Ωm at 420 K. Using both methods AC and DC measurements, for resistivities for different fibers are in good agreement with each other.

For temperature sensing purposes, a parameter called sensitivity α can be defined, which is the negative slope of resistivity divided by resistivity at 300 K ($\alpha = -\text{Slope}/\rho_{(300\,\text{K})}$) (Table 2). The most significant value presents the sample reduced at 120 °C

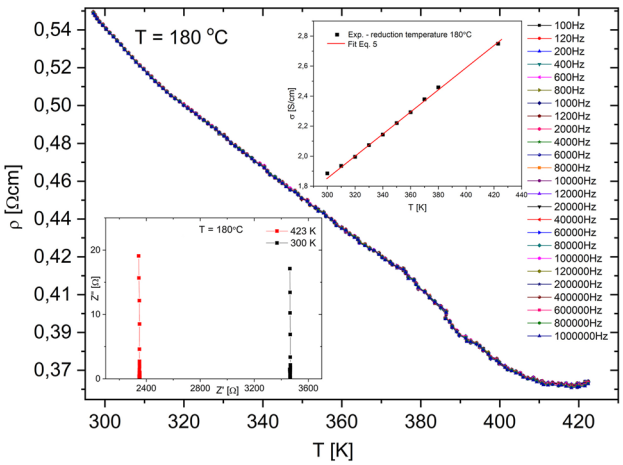

Fig. 5 AC resistivity vs. temperature for the frequency range 100 Hz–1 MHz; (inset right) DC conductivity estimated from AC data (for 0 Hz) vs. reduction temp. (300–423 K); (inset, left) Nyquist plot for sample reduced at 180 °C (453 K) measured 300 and 423 K

Table 2 The slope taken from linear fit at temp 300 K and sensitivity α

Reduction temp [°C]	Slope at 300 K [Ωcm/°C]	α[°C^{-1}]
120	− 357.4 ± 11.1	139.1
130	− 11.71 ± 0.28	48.8
140	− 8.85 ± 0.39	40.2
150	− 15.32 ± 2.09	42.6
160	− 10.99 ± 0.33	35.5
170	− 8.03 ± 0.38	13.6
180	− 13.18 ± 0.57	24.4
190	− 42.3 ± 1.7	21.7

(~ 140 °C^{-1}), and simultaneously, it shows the largest resistivity. Compared with other carbon materials, this parameter can reach 1700 K^{-1} [40], making them much more suitable for sensing. Reducing GO at higher temperatures decreases the resistivity and α parameter altogether.

Figure 5 shows the AC data collected for frequencies from 100 Hz to 1 MHz for samples reduced at 180 °C and dried before measurements. Other samples show similar linear temperature dependence, although shifted towards higher resistivities.

Due to the heat treatment, which removed most entrapped water before measurement, the conductivity is purely caused by electrons (Fig. 5, inset). The Nyquist plot shows no semi-circle behavior typical for ionic transporting samples that would occur if entrapped in pores' water ions would have taken part in the conductivity process.

4 Conclusions

The electrical conductivity model showing the highest fidelity described by the R^2 parameter utilizes two mechanisms described by Mott VRH ($\beta = 1/3$) for lower temperatures and Efros-Shklovskii VRH ($\beta = 0.5$) for higher temperatures ($R^2 = 0.9997$ and 0.9994, respectively). This combination of mechanisms outperformed a single-type conductivity model in our study.

The sample reduced at 120 °C (393 K) exhibits higher resistivity due to the more significant presence of oxygen groups and loose pore structure, leading to higher electron scattering. The sample shows the largest water content, visible in the difference between room temperature and after-drying resistivity. 120 °C is simultaneously the lowest reduction temperature at which rGO fiber was successfully formed. In the temperature range of 130–180 °C, samples show a slight decrease in resistivity caused by rising reduction temperature. Magnetoresistivity studies in 0, 0.5, and 1 T have shown no qualitative differences in the resistivities measured with and without an external magnetic field. This, although indirect, informs of a lack of iron and manganese particles, as well as other metals, which could be contamination stemming from the Hummers method used for obtaining GO or even previous contamination of graphite used. The most considerable sensitivity parameter α shows the sample reduced at 120°C with the α value ~ 140 °C^{-1}. Samples with lower resistivity show weaker resistivity dependence on temperature.

Author contributions

Adam Ostrowski—AC electrical measurements, writing and correcting the article. Karol Synoradzki—DC electrical measurements, magneto resistivity measurements, data evaluation, writing and correcting the article. Damian Tomaszewski—data evaluation, literature research, writing and correcting the article. Krzysztof Tadyszak—preparation of samples, SEM, EDX, data evaluation, writing and correcting the article.

Funding

Open access publishing supported by the National Technical Library in Prague. We acknowledge the financial support from the Ministry of Education, Youth and Sports of the Czech Republic (grants # LM2023053 and LUAUS24272) and the National Science Centre of Poland (Grant no. 2020/36/C/ST3/00539).

Data availability

Data will be made available at a reasonable request.

Declarations

Conflict of interest There are no conflicts of interest to declare.

References

1. A. Colburn, N. Wanninayake, D.Y. Kim, D. Bhattacharyya, Cellulose-graphene quantum dot composite membranes using ionic liquid. J. Membr. Sci. **556**, 293 (2018). https://doi.org/10.1016/j.memsci.2018.04.009
2. S. Takahashi, R. Hanson, J. van Tol, M.S. Sherwin, D.D. Awschalom, Quenching spin decoherence in diamond through spin bath polarization. Phys. Rev. Lett. **101**, 047601 (2008). https://doi.org/10.1103/PhysRevLett.101.047601
3. Z. Xu, H. Sun, X. Zhao, C. Gao, Ultrastrong fibers assembled from giant graphene oxide sheets. Adv. Mater. **25**, 188 (2013). https://doi.org/10.1002/adma.201203448
4. S.H. Kim, C.S. Haines, N. Li et al., Harvesting electrical energy from carbon nanotube yarn twist. Science **357**, 773 (2017). https://doi.org/10.1126/science.aam8771
5. K. Kostarelos, K.S. Novoselov, Exploring the interface of graphene and biology. Science **344**, 261 (2014). https://doi.org/10.1126/science.1246736
6. D. Mircea, G. Lidia, O. Cosmin et al., Ultra-lightweight pressure sensor based on graphene aerogel decorated with piezoelectric nanocrystalline films. Nanotechnology **27**, 475203 (2016)
7. A. González-Mayorga, E. López-Dolado, M.C. Gutiérrez et al., Favorable biological responses of neural cells and tissue interacting with graphene oxide microfibers. ACS Omega **2**, 8253 (2017). https://doi.org/10.1021/acsomega.7b01354
8. S.S. Yoon, K.E. Lee, H.-J. Cha et al., Highly conductive graphene/Ag hybrid fibers for flexible fiber-type transistors. Sci. Rep. **5**, 16366 (2015). https://doi.org/10.1038/srep16366
9. X. Zhao, B. Zheng, T. Huang, C. Gao, Graphene-based single fiber supercapacitor with a coaxial structure. Nanoscale **7**, 9399 (2015). https://doi.org/10.1039/C5NR01737H
10. B.J. Kim, H. Jang, S.-K. Lee, B.H. Hong, J.-H. Ahn, J.H. Cho, High-performance flexible graphene field effect transistors with ion gel gate dielectrics. Nano Lett. **10**, 3464 (2010). https://doi.org/10.1021/nl101559n
11. Y. Shao, J. Wang, H. Wu, J. Liu, I.A. Aksay, Y. Lin, Graphene-based electrochemical sensors and biosensors: a review. Electroanalysis **22**, 1027 (2010). https://doi.org/10.1002/elan.200900571
12. B. Piro, G. Mattana, S. Zrig et al., Fabrication and use of organic electrochemical transistors for sensing of metabolites in aqueous media. Appl. Sci. **8**, 928 (2018)
13. VP Vasiliev, VA Smirnov (2019) A review on the conductive properties of graphene oxide Films. Int. J. Adv. Res. Chem. Sci.
14. Y. Jin, W. Lee, Cross-linking stabilizes electrical resistance of reduced graphene oxide in humid environments. Langmuir **35**, 5427 (2019). https://doi.org/10.1021/acs.langmuir.8b03416
15. V.B. Mohan, R. Brown, K. Jayaraman, D. Bhattacharyya, Characterisation of reduced graphene oxide: effects of reduction variables on electrical conductivity. Mater. Sci. Eng. B **193**, 49 (2015). https://doi.org/10.1016/j.mseb.2014.11.002
16. M.A. Augustyniak-Jabłokow, R. Strzelczyk, R. Fedaruk, Localization of conduction electrons in hydrothermally reduced graphene oxide: electron paramagnetic resonance studies. Carbon **168**, 665 (2020). https://doi.org/10.1016/j.carbon.2020.07.023
17. K. Tadyszak, R. Strzelczyk, E. Coy, M. Maćkowiak, M.A. Augustyniak-Jabłokow, Size effects in the conduction electron spin resonance of anthracite and higher anthraxolite. Magn. Reson. Chem. **54**, 239 (2016). https://doi.org/10.1002/mrc.4373
18. S. Wu, R.B. Ladani, J. Zhang et al., Strain sensors with adjustable sensitivity by tailoring the microstructure of graphene aerogel/PDMS nanocomposites. ACS Appl. Mater. Interfaces **8**, 24853 (2016). https://doi.org/10.1021/acsami.6b06012
19. Ł Majchrzycki, M.A. Augustyniak-Jabłokow, R. Strzelczyk, M. Máckowiak, Magnetic centres in functionalized graphene. Acta Phys. Pol. A **127**, 540 (2015)
20. K. Tadyszak, A. Musiał, A. Ostrowski, J.K. Wychowaniec, Unraveling origins of EPR spectrum in graphene oxide quantum dots. Nanomaterials **10**, 798 (2020)
21. W. Park, J. Hu, L.A. Jauregui, X. Ruan, Y.P. Chen, Electrical and thermal conductivities of reduced graphene oxide/polystyrene composites. Appl. Phys. Lett. (2014). https://doi.org/10.1063/1.4869026
22. C. Gómez-Navarro, R.T. Weitz, A.M. Bittner et al., Electronic transport properties of individual chemically reduced graphene oxide sheets. Nano Lett. **7**, 3499 (2007). https://doi.org/10.1021/nl072090c
23. D. Joung, S.I. Khondaker, Efros-Shklovskii variable-range hopping in reduced graphene oxide sheets of varying carbon sp^2 fraction. Phys. Rev. B **86**, 235423 (2012). https://doi.org/10.1103/PhysRevB.86.235423

24. C. Chuang, R.K. Puddy, H.D. Lin et al., Experimental evidence for Efros-Shklovskii variable range hopping in hydrogenated graphene. J Solid State Commun. **152**, 905 (2012)
25. K. Tadyszak, Ł. Majchrzycki, Ł. Szyller, B. Scheibe, Preparation and characterization of partially reduced graphene oxide aerogels doped with transition metal ions. J. Mater. Sci. **53**, 16086 (2018). https://doi.org/10.1007/s10853-018-2770-x
26. K. Tadyszak, J.K. Wychowaniec, K. Załęski, E. Coy, Ł. Majchrzycki, R. Carmieli, Tuning properties of partially reduced graphene oxide fibers upon calcium doping. Nanomaterials **10**, 957 (2020)
27. K. Tadyszak, B. Wereszczyńska, M. Gonet, CT, MR and EPR imaging of graphene oxide aerogels. Solid State Sci. **109**, 106402 (2020). https://doi.org/10.1016/j.solidstatesciences.2020.106402
28. C. Botas, P. Álvarez, C. Blanco et al., Critical temperatures in the synthesis of graphene-like materials by thermal exfoliation-reduction of graphite oxide. Carbon **52**, 476 (2013). https://doi.org/10.1016/j.carbon.2012.09.059
29. W. Guo, X. Zhang, X. Yu et al., Self-powered electrical stimulation for enhancing neural differentiation of mesenchymal stem cells on graphene–poly(3,4-ethylenedioxythiophene) hybrid microfibers. ACS Nano **10**, 5086 (2016). https://doi.org/10.1021/acsnano.6b00200
30. Z. Dong, C. Jiang, H. Cheng et al., Facile fabrication of light flexible and multifunctional graphene fibers. Adv. Mater. **24**, 1856 (2012). https://doi.org/10.1002/adma.201200170
31. K. Tadyszak, B. Scheibe, A. Ostrowski, A. Musiał, J.K. Wychowaniec, Influence of thermochemical reduction on magnetic properties of reduced graphene oxide aerogels. J. Phys. Chem. Solids **151**, 109898 (2021). https://doi.org/10.1016/j.jpcs.2020.109898
32. R. Bakhtiari, S. Ghobadi, E.N. Güllüoğlu, L.I. Şanlı, S.A. Gürsel, E. Özden-Yenigün, Macroscopic assembly of flexible and strong green graphene fibres. RSC Adv. **7**, 26735 (2017). https://doi.org/10.1039/C7RA03975A
33. Q. Su, S. Pang, V. Alijani, C. Li, X. Feng, K. Müllen, Composites of graphene with large aromatic molecules. Adv. Mater. **21**, 3191 (2009). https://doi.org/10.1002/adma.200803808
34. J.U. Lee, W. Lee, J.W. Yi et al., Preparation of highly stacked graphene papers via site-selective functionalization of graphene oxide. J. Mater. Chem. A **1**, 12893 (2013). https://doi.org/10.1039/C3TA11717K
35. E.A.D. Nevill, F. Mott, *Electronic Processes in Non-Crystalline Materials* (Oxford University Press, New York, 2012)
36. J. Robertson, Amorphous carbon. Adv. Phys. **35**, 317 (1986). https://doi.org/10.1080/00018738600101911
37. G. Eda, C. Mattevi, H. Yamaguchi, H. Kim, M. Chhowalla, Insulator to semimetal transition in graphene oxide. J. Phys. Chem. C **113**, 15768 (2009). https://doi.org/10.1021/jp9051402
38. D. Kong, L.T. Le, Y. Li, J.L. Zunino, W. Lee, Temperature-dependent electrical properties of graphene inkjet-printed on flexible materials. Langmuir **28**, 13467 (2012). https://doi.org/10.1021/la301775d